Angular and frequency spectral analysis of the ultrasonic backward beam displacement on a periodically grooved solid

Sarah W. Herbison[a] and Nico F. Declercq
George W. Woodruff School of Mechanical Engineering, Georgia Institute of Technology, 801 Ferst Drive, Atlanta, Georgia 30332-0405 and Laboratory for Ultrasonic Nondestructive Evaluation, Georgia Tech Lorraine, GT-CNRS UMI 2958, 2-3 rue Marconi, 57070 Metz, France

Mack A. Breazeale
National Center for Physical Acoustics, The University of Mississippi, Oxford, Mississippi 38677

(Received 28 November 2008; revised 10 September 2009; accepted 15 September 2009)

The ultrasonic backward beam displacement, which has been shown to occur when a bounded beam is incident upon a periodically corrugated liquid-solid interface, is studied experimentally. This effect has been previously studied on a periodic water-brass interface at one particular frequency (6 MHz) and one corresponding angle of incidence (22.5°), but the question has remained whether it would also exist at other frequency and angle combinations. The knowledge of whether this phenomenon is a coincidence or whether it will occur for other frequency and angle combinations contributes to a better understanding of the interaction of ultrasound with periodic structures and diffraction effects, in particular. Potential applications exist in the study of phononic crystals and in the non-destructive evaluation of materials. The present work reports results from recent experiments on the same periodically grooved brass sample that was employed in the first investigations of this phenomenon. Through the examination of frequency spectra in the form of angular and classical spectrograms, the experiments reported here show the backward beam displacement to occur for multiple angles of incidence and frequencies. Furthermore, evidence is shown as to the exact cause of the backward beam displacement, namely, a backward propagating Scholte–Stoneley wave. © *2009 Acoustical Society of America.* [DOI: 10.1121/1.3243467]

PACS number(s): 43.35.Bf, 43.30.Hw, 43.20.El, 43.35.Pt [RR] Pages: 2939–2948

I. INTRODUCTION

The ultrasonic backward beam displacement on a periodically corrugated surface, as shown in Fig. 1(a), has intrigued scientists since the 1970s when it was initially discovered by Breazeale and Torbett.[1] The motivation behind their work was to discover the acoustic phenomenon that would correspond to the optical phenomenon predicted by Tamir and Bertoni, where an interface with a periodic structure superimposed may cause a leaky wave to propagate in the backward direction, resulting in a backward displacement of the specularly reflected beam.[2] Using schlieren imaging and a bounded beam with a frequency of 6 MHz at an angle of incidence of 22.5°, Breazeale and Torbett did indeed observe the first ultrasonic backward beam displacement, as shown in Fig. 1(b).

Although the phenomenon was of physical interest from the time of its discovery, the backward beam displacement did not receive attention in the 1980s and 1990s when periodically corrugated surfaces were being used to transform bulk waves into surface waves for the non-destructive testing of surfaces of materials because at that time the focus was on the study of normal, and not oblique, incidence.[3] However, the interaction of sound with periodic structures, periodic surfaces being but one example, has attracted new interest in the past decade with the study of phononic crystals.[4–7] Due to the unique properties that stem from their periodicity (band gaps, etc.), these acoustic counterparts of photonic crystals in optics have potential applications including acoustic filtering and novel transducers.[8,9] In addition, periodic surfaces have recently been investigated in the context of Lamb wave propagation in corrugated plates (waveguides) with applications in the non-destructive evaluation of non-planar surfaces[10] and surface roughness characterization.[11]

Also in recent years, the backward beam displacement has received new attention with the proposal of a numerical technique by Declercq *et al.*[12] based on a combination of inhomogeneous wave theory and the Rayleigh theory of diffraction that enabled the simulation of the beam displacement. The same theoretical approach was then used to study the effect of the beam width and to reveal the cause of the effect, which turned out to be a leaky form of Scholte–Stoneley waves.[13] Shortly thereafter, experiments were conducted by Teklu *et al.*[14] that showed agreement with theoretical predictions concerning the influence of the beam width. Their experiments using schlieren photography also showed that the backward beam shift appeared when the negative first order diffracted sound beam was barely visible along the surface of the sample. This observation was considered a signal of the transition of the negative first order from a bulk wave to a Scholte–Stoneley wave with decreasing angle of

[a]Author to whom correspondence should be addressed. Electronic mail: sherbison@gatech.edu

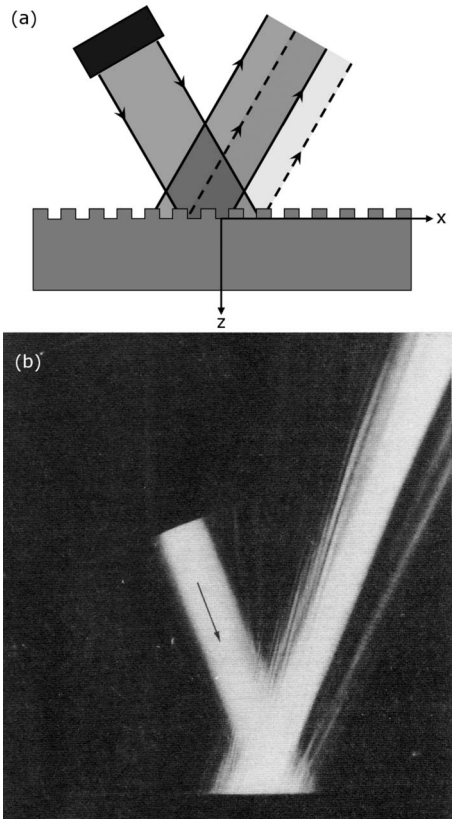

FIG. 1. (a) Diagram of the ultrasonic backward beam displacement on a periodically corrugated surface. The location of the specular beam predicted geometrically is shown by dashed lines. The backward shifted beam is shown in solid lines. The backward propagating leaky surface wave causing the beam shift propagates in the negative x-direction. Corrugation profile enlarged for illustration. (b) Schlieren image showing the backward displacement of a 6 MHz ultrasonic beam on a water-brass grating interface (Ref. 1).

incidence, but there was no hard evidence. (It should be noted that on homogeneous, planar solid surfaces, phase matching considerations prevent the coupling between bulk waves and Scholte–Stoneley waves. However, in the case of a homogeneous non-planar solid surface such as the periodically corrugated one studied in this work, a coupling between bulk waves and Scholte–Stoneley waves can exist.[15])

Prior to this experimental work by Teklu *et al.*, a numerical study on the behavior of Scholte–Stoneley waves when they encounter the corner of a solid plate[16] revealed that Scholte–Stoneley waves are scattered in the forward direction upon reaching the corner and do not propagate around the corner in the manner of leaky Rayleigh waves.[17,18] This phenomenon has also been shown experimentally.[19]

The present work has two objectives, both accomplished experimentally. The first objective is to quantitatively show that the backward beam displacement exists at additional frequencies and angles of incidence other than the single frequency and angle of incidence pair (6 MHz, 22.5°) studied in the past and to show that the classical grating equation can be used to theoretically predict potential frequency and angle pairs. The second objective is to show that the backward displacement is accompanied by a backward propagating Scholte–Stoneley wave, which results in the known transmission effect upon reaching the edge of the solid sample. This work realizes both of these objectives through the analysis of frequency spectra resulting from angular scans of the ultrasound fields in water using a newly developed polar/C-scan apparatus at Georgia Tech Lorraine. All the experiments reported here are performed on the original grooved brass sample that was used in 1976 when Breazeale and Torbett[1] first reported the ultrasonic backward beam displacement.

II. THEORETICAL CONSIDERATIONS

We consider a bounded beam incident from water (with a sound velocity v_{liq}) at an angle of incidence θ_i onto a grooved solid surface with spatial periodicity Λ. All angles of incidence are given from the normal to the surface, and the beam is considered to be time-harmonic with frequency f. From the classical diffraction grating equation,[2] an expression is formulated that gives the optimum angle of incidence for the generation of a diffracted backward propagating lateral wave (e.g., surface wave with velocity v_{surf}):

$$\sin(\theta_i) = v_{\mathrm{liq}}\left(\frac{1}{f\Lambda} - \frac{1}{v_{\mathrm{surf}}}\right). \tag{1}$$

This expression can be inverted to give the frequency of the backward propagating lateral wave given a known angle of incidence. [In the derivation of Eq. (1), the diffracted surface wave generated is considered to be of the negative first order since higher order modes will not propagate for the frequencies and surface periodicity examined in this work.] It was predicted by Tamir and Bertoni[2] that the presence of a backward propagating leaky wave would interfere with the specularly reflected beam and result in its lateral backward displacement. In the first investigation of this prediction, Breazeale and Torbett used a value of 2015 m/s, the leaky Rayleigh wave velocity on brass, as the velocity of the backward propagating leaky surface wave and a velocity of 1490 m/s for water. Their sample had a rectangular corrugation profile with a periodicity of 178 μm and a height of 25 μm. The length of the grooved portion of the sample was 25.4 mm. The result of their calculation was a prediction of 41° for the optimal angle of incidence to generate the backward displacement for an incident beam with a frequency of 6 MHz. However, their experiments using schlieren photography showed that the backward displacement occurred for their beam at an angle of incidence of $22.5° \pm 0.25°$, not 41° as predicted. This suggested that either the theory of Tamir and Bertoni did not accurately describe the backward beam displacement or that the surface wave responsible for the phenomenon was not, in fact, a leaky Rayleigh wave.

As discussed in the Introduction, it was later shown that the angle at which the backward beam displacement appears can be predicted by the knowledge that the effect is induced by a leaky type of backward propagating Scholte–Stoneley wave.[13] With this knowledge, calculations show that the surface wave responsible for the backward displacement of the 6 MHz beam incident at $22.5° \pm 0.25°$ on the grooved brass sample of Breazeale and Torbett would have a velocity between 1465.8 and 1477.6 m/s with an average of 1471.7 m/s.

Even though, in general, one may expect dispersion of Scholte–Stoneley waves on corrugated surfaces and a dependence of the velocity on the corrugation periodicity, this velocity can be used as a basis in order to predict the angle of incidence and frequency pairs at which one may expect the backward beam displacement to appear on the surface under study. Thus, the frequency and angle pairs predicted by Eq. (1), with a Scholte–Stoneley wave velocity of 1471.7 m/s used as v_{surf}, will be compared to the frequency and angle pairs observed experimentally in this work. In addition, the velocity of sound in the water used for the recent experiments reported here was measured to be 1479.5 m/s, and we will use this velocity as v_{liq} in Eq. (1) in order to be consistent with the actual experimental environment.

In addition to predicting the frequency and angle of incidence combinations that should result in the backward beam displacement and the generation of a backward propagating Scholte–Stoneley wave, the classical grating equation also provides information on the propagation of diffracted bulk modes that are not confined to the surface of the sample. In prior studies of the backward beam displacement, only single frequency beams (i.e., time-harmonic ultrasonic beams) have been employed, and so the presence of the backward propagating Scholte–Stoneley wave was examined without the possibility of other propagating bulk modes being present. However, in this study an ultrasonic pulse is employed so that many frequencies can be examined simultaneously. This results in the presence of additional propagating bulk modes in the fluid that are not confined to the vicinity of the surface of the sample; this occurs only for frequencies that are higher than the frequency of the backward Scholte–Stoneley wave generated at a given angle of incidence. The propagating bulk modes are also considered to be of the negative first order and their angles of propagation, θ_{pm}, can be predicted by the following expression, also derived from the classical grating equation:

$$\sin\,\theta_{pm} = \frac{v_{liq}}{f\Lambda} - \sin\,\theta_i. \tag{2}$$

Using Eq. (2) for an ultrasonic pulse at a given angle of incidence, the directions of the propagating modes for many frequencies can be predicted.

III. EXPERIMENTAL SETUP

A single experimental setup is used to accomplish both of the objectives of this work as described in the Introduction. All measurements are performed underwater in an ultrasonic immersion tank. The experimental setup consists of a pitch-catch arrangement with a stationary transducer emitting a pulse with a center frequency equal to approximately 5 MHz that is incident upon the grooved brass sample. The propagation distance between the incident transducer and the sample is 66 mm, and the beam width is approximately 12 mm. The beam used in the original experiments of Breazeale and Torbett was 10 mm in width, and it was shown by Teklu *et al.*[14] that the backward displacement is not necessarily visible for smaller beam widths. The incident pulse and its frequency spectrum are shown in Fig. 2. The diffracted fields

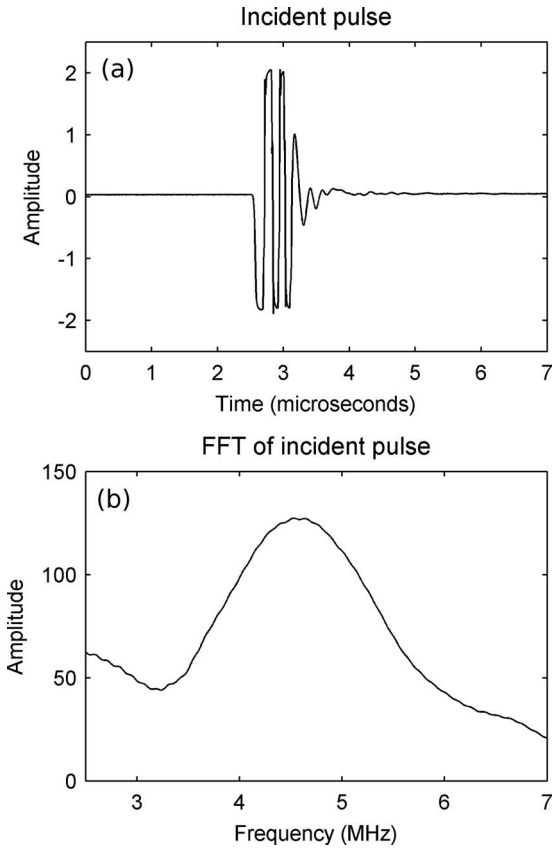

FIG. 2. (a) Time waveform of the incident pulse and (b) its frequency spectrum.

generated by the sample are scanned with a receiving transducer that rotates about the point of incidence on the sample surface. This transducer is mounted in the polar/C-scan apparatus which controls the rotation of the scan and the timing of the waveform acquisition. The distance between the sample and the receiving transducer is chosen to be 45 mm in order to be compatible with the rotation of the polar/C-scan equipment. The receiving transducer is continuously aimed at the point of incidence on the grooved sample and the propagation distance remains unchanged during rotation. In order to change the angle of incidence, the sample is mounted in such a manner that it can be rotated. A photograph of the experimental setup (before submersion in the tank) is shown in Fig. 3, with the sample rotated such that the beam from the emitting transducer would be normally incident to the sample surface.

Two types of scans are performed. The first scans the diffracted field in front of the emitting transducer (where the specularly reflected beam and any backward shifted frequencies would be present) in order to quantitatively observe the backward beam shift. A schematic of this scan is shown in Fig. 4(a). A scan is performed each time the angle of incidence is changed (clockwise rotation of the sample). The angular resolution is 0.25° and the angular range is 70° for all scans. The start and end points of each scan are determined by geometrical constraints and so their locations with respect to the polar/C-scan equipment are identical for all scans.

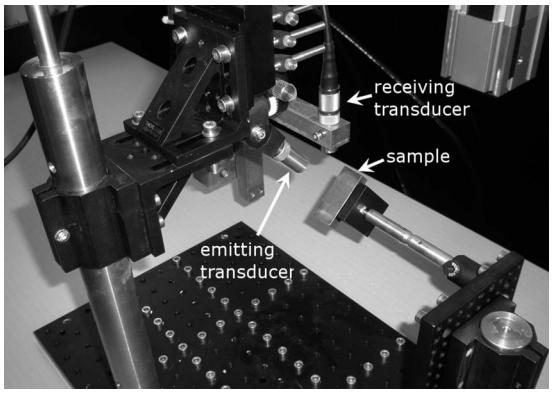

FIG. 3. Photo of the experimental setup with the sample rotated such that the beam from the emitting transducer is normally incident upon the sample. Photo was taken before submersion in the water tank.

The second type of scan measures the diffracted field behind the emitting transducer (near the surface of the sample where the backward propagating surface wave is predicted to be found) in order to quantitatively observe the backward propagating surface wave that is predicted to accompany the backward beam displacement. To scan this area of the diffracted field, the sample is rotated in the opposite (counter-clockwise) direction so that the receiving transducer is now in the field considered to be behind the emitting transducer. A schematic of this scan is shown in Fig. 4(b). A scan

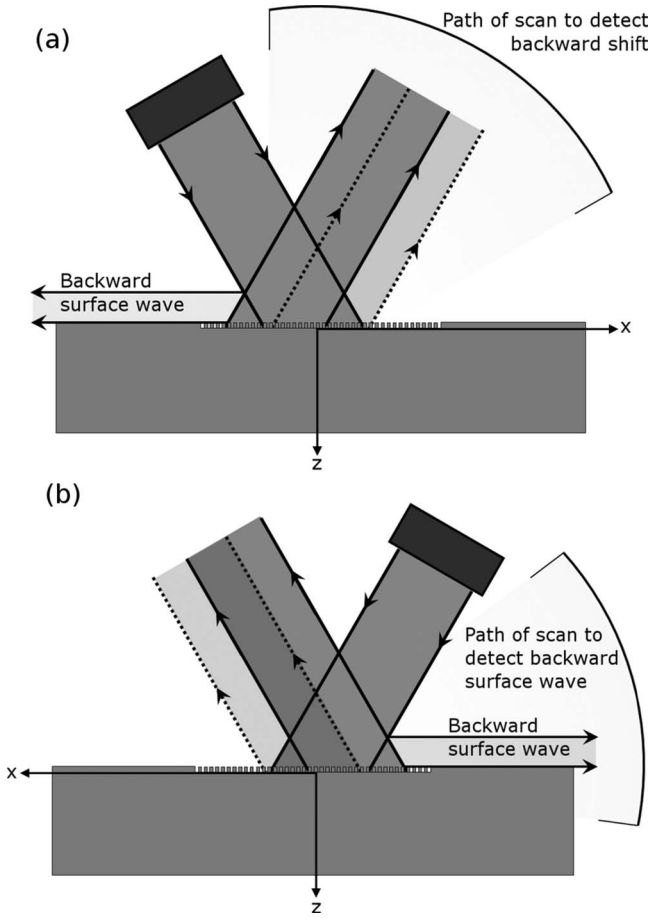

FIG. 4. (a) Scan path to detect the backward beam shift. (b) Scan path to detect the backward propagating Scholte–Stoneley wave.

is performed each time the sample is rotated to change the angle of incidence. The angular resolution and angular range of these scans are also 0.25° and 70°, respectively.

The measurements for the angles of incidence (i.e., angles of rotation of the sample) given in this work should be considered as accurate to ±1°. Before we report our experimental results, it is appropriate to discuss a consequence of the rotational nature of our scans, namely, their sensitivity to the magnitude of the backward displacement along the surface and to the angle of incidence (or rather specular reflection). The backward beam displacement is considered to be a lateral shift of a (time-harmonic) beam along the surface. However, in this work, as the beam employed is a pulse, we expect only a single or very narrow range of frequencies to be shifted backward while all other frequencies within the pulse will remain in the specularly reflected beam. For a constant angle of incidence, as the magnitude of the lateral shift of the backward displaced frequencies increases and moves away from the specularly reflected beam, their detection becomes more difficult since this backward shifted portion becomes less normal to the surface of the receiving transducer during the scan. For a constant magnitude of the lateral shift, the backward displaced portion of the beam at small angles of incidence will be less normal to the surface of the receiving transducer (and thus its detected amplitude will be lower than the reality) than it would be for larger angles of incidence as it rotates through the scan. In addition, this given lateral shift along the surface will also be more difficult to detect if it occurs for a too large angle of incidence. It should be noted that the receiving transducer does not detect the lateral shift of the backward displaced portion of the beam, but rather the projection of that lateral shift at the transducer surface. As the angle of incidence increases, the projection of the lateral shift and hence the distance between the backward displaced and the specularly reflected portions of the beam decreases at the surface of the transducer. The lateral shift then becomes more difficult to detect since it is seen as part of the specular beam.

The conclusion of this discussion is that using the rotational scans as described in this work, the backward beam displacement can be best detected within a middle range of angles of incidence. It should also be noted that even though these effects should be taken into account when using a rotational scan to measure the backward beam displacement, this type of scan is an ideal tool to measure both the backward propagating surface wave and the propagating modes that occur behind the emitting transducer, simultaneously.

IV. RESULTS

The earlier experiments reported by Breazeale and Torbett[1] and by Teklu *et al.*[14] studied the interaction of continuous time-harmonic waves with the corrugated brass sample using schlieren imaging. However, the experiments of this work employ a pulse in order to study many frequencies, all of which are simultaneously incident on the sample. To separate the different frequencies, a Fourier transformation is performed on the detected signals after their acquisition. First, the original observations of Breazeale and Torbett

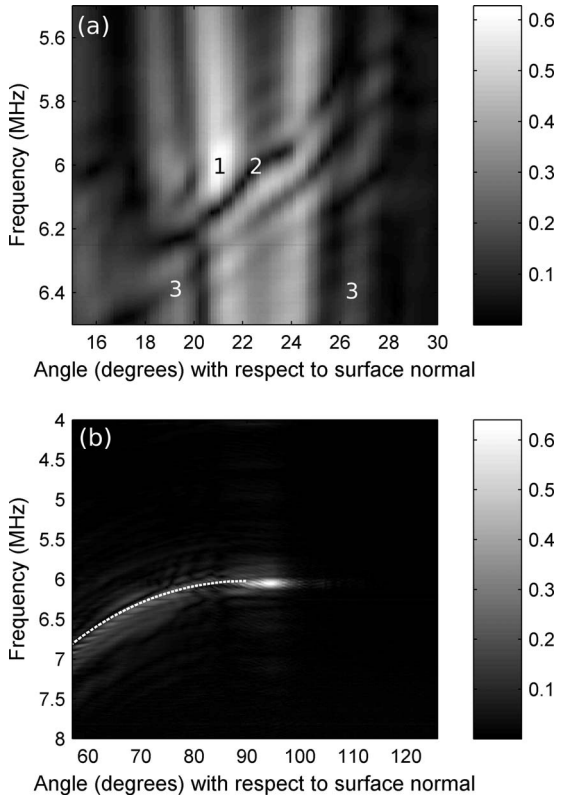

FIG. 5. Angular spectrograms confirming the results obtained by Breazeale and Torbett. For a θ_i of 22.5°, a spectrogram from the region of the specularly reflected beam (a) shows a null zone of frequencies in the range 5.95–6.16 MHz. The complementary spectrogram from a scan to detect the backward surface wave (b) shows it occurring at 6.05 MHz. Propagating bulk modes also detected in (b) and shown theoretically by dotted line.

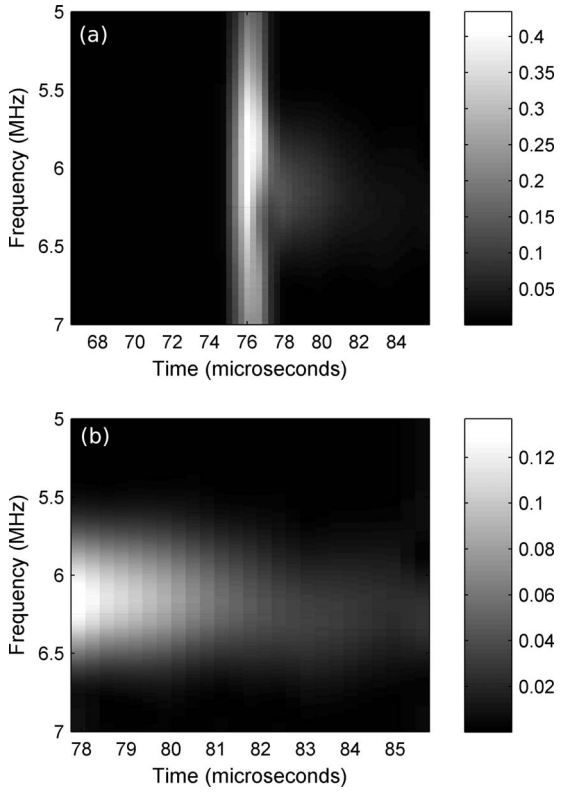

FIG. 6. (a) Classical spectrogram for a θ_i of 22.5° obtained from the time waveform captured at a receiver angle of 21°. (b) Close-up of the classical spectrogram in (a) to show the trailing frequencies arriving after the initial pulse.

are studied using the current experimental method. We next discuss the results obtained for additional angles of incidence and frequencies. Results are reported in the form of angular spectrograms, which show the amplitude of frequencies present in the waveform detected by the receiving transducer as a function of the angle of the transducer within the field. In addition, classical spectrograms, which show frequencies present in the time waveform detected by the receiving transducer as a function of time, are presented.

In what follows, all results are normalized with respect to the frequency spectrum of the incident beam. The angular spectrograms, then, are amplitude plots as a function of frequency and position. They are not schlieren-type images, but are measurements in the plane of interaction at a certain radius from the interaction spot.

A. Confirmation of the observations of Breazeale and Torbett

For a θ_i of 22.5°, a scan of the region of the specularly reflected beam results in the angular spectrogram shown in Fig. 5(a). The beam is centered at the angle of specular reflection, 22.5°, as expected. There are also three note-worthy features within this angular spectrogram, and they are numbered on Fig. 5(a).

First, there is a bright zone of frequencies with higher amplitudes, labeled as "1" in Fig. 5(a), centered approximately at an angular position of 21° and at a frequency of 6 MHz. If we examine the angular spectrogram closely, the maximum amplitude within this zone is found to be at an angular position of 21° and at a frequency of 5.98 MHz. Frequencies having high amplitudes (greater than 0.55) within the bright zone exist between 5.92 and 6.08 MHz, and frequencies within this range do not have such high amplitudes on the opposite side of the beam. The existence of this high-amplitude bright zone indicates that the energy from frequency components in this range is not distributed equally from left to right across the beam profile; these frequencies are disproportionately found on the left side. This result can be interpreted as evidence of these frequencies having been shifted backward. However, if this is indeed the case, these frequencies should be seen to have a later arrival time in a classical spectrogram.

Therefore, a classical spectrogram was obtained from the time waveform captured at a receiver position of 21°, and it is shown in Fig. 6(a). If the backward beam displacement occurs as it is currently understood, a frequency component that is shifted backward should arrive after the other non-shifted frequencies in the beam. This is due to finite nature of wave propagation speeds; any frequency that is shifted backward with respect to the specular direction must first travel backward along the surface at the speed of the backward propagating surface wave before re-radiating from the sample surface to the receiving transducer. When we examine this classical spectrogram, we see the arrival of the specular beam (a pulse) as a solid vertical band of frequencies. The time duration of the pulse as it is seen by the

receiving transducer is a function of the beam width, the angle of incidence, and the incident pulse duration. However, this specular beam arrival is followed by a faint trail of frequencies that can be seen more clearly in Fig. 6(b). In this close-up of Fig. 6(a), a band of "trailing" frequencies is seen to arrive after the initial pulse. The band of trailing frequencies is quite wide, and the frequency of maximum amplitude of the band is 6.17 MHz along many of the initial time windows of the spectrogram.

Returning to the angular spectrogram in Fig. 5(a), the second note-worthy feature is the presence of a null zone (with amplitudes less than 0.1), labeled as "2" in the figure, inside the specular beam. This null zone represents frequencies at positions between 20.75° and 23.75° that are detected as having very low amplitudes in the angular scan. The frequencies in the null zone range from 6.15 to 6.16 MHz at 20.75° and from 5.95 to 5.96 MHz at 23.75°. The existence of this null zone is most likely due to phase cancellation between specularly reflected sound and re-radiated (backward shifted) sound. The presence of null strips due to phase cancellation in the reflected fields generated by incident bounded beams, such as those seen in studies of the Schoch effect, are well documented.[20,21]

Finally, we note the presence of vertical bands showing many frequencies present to the left and right of the specular beam, namely, at angles of 19° and 26.5° and labeled as "3" in Fig. 5(a). The vertical bands to the left and right of the specular beam can be attributed to deformation of the beam that occurs upon reflection, which is not an uncommon occurrence especially in the case of periodically corrugated surfaces. Such beam deformation and beam widening, in particular, can be seen in several references. In particular, Figs. 5 and 6 in the work of Teklu *et al.*[14] show the deformation of an ultrasonic beam upon reflection from a periodically corrugated surface. Specular beam deformation is also seen in the original schlieren image of the ultrasonic backward beam displacement observed by Breazeale in 1976[1] that we have shown in Fig. 1.

The spectrogram of the complementary scan in the region of the backward propagating surface wave for the same angle of incidence, 22.5°, is shown in Fig. 5(b). Here a backward propagating surface wave with an amplitude maximum at a frequency of 6.05 MHz can be seen with a range of frequencies surrounding the amplitude maximum. This angular spectrogram shows that the backward propagating surface wave propagated directly off the surface of the sample and into the field of the receiving transducer, as one would expect from a Scholte–Stoneley wave. Higher frequency propagating bulk orders are also seen in the spectrogram of Fig. 5(b). The dotted line plotted on the spectrogram corresponds to the theoretical angles of the propagating bulk modes as a function of frequency, calculated from Eq. (2). The presence of faint additional frequencies at the same angular position as the backward propagating Scholte–Stoneley wave can be explained as being evanescent waves, negative first order for frequencies below the Scholte–Stoneley frequency or higher order for higher frequencies.

A summary of these results is the following. From the scan in the region of the specular beam, it is clear that there is an imbalance of frequencies across the beam profile from left to right for frequencies in the vicinity of 6 MHz (± 0.08 MHz). There is also a null zone consisting of a band of frequencies between 5.95 and 6.15 MHz depending on the angle of the receiver. From the classical spectrogram, it is seen that at a receiver angle of 21°, left of the center of the specular beam, a wide band of frequencies with a maximum at 6.17 MHz arrives after the specular beam. This band of trailing frequencies is sufficiently wide as to include frequencies in both the high-amplitude bright zone and the null zone in the angular spectrogram. From the scan in the region behind the incident beam, a backward propagating surface wave with an amplitude maximum at a frequency of 6.05 MHz was detected.

From this evidence, we are led to conclude that the null zone in the center of the specular beam is likely due to phase cancellation resulting from those frequencies having been shifted backward. This is based on the observation that many of the frequencies in the null zone can be located in the bright zone centered at 21° and that in the classical spectrogram taken from the time waveform arriving at 21°, the band of frequencies arriving after the specular beam contains all of the frequencies in the null zone. For those frequencies appearing in the null zone (located below the bright zone) at a receiver location of 21°, we suspect that they have been shifted backward as well, but since the sensitivity of the receiving transducer decreases dramatically for sound not normally incident to its surface, it is possible that this became an issue at the angles where these frequencies could have been detected.

All prior studies on the ultrasonic backward beam displacement have employed a time-harmonic beam, not a pulse. Therefore, when a pulse is employed, there exists the possibility that for a given angle of incidence there is actually a range of frequencies, and not just a single frequency, that can be shifted backward. We make this hypothesis based on the observation that in the classical spectrogram of Fig. 6(b), it is a fairly wide band of frequencies that arrives after the specular beam. This result could also be due to imperfections on the corrugated surface. One particularly interesting feature of this band of trailing frequencies is its duration: we can see for how long these frequencies continue to arrive at the receiving transducer, which provides insight into the time-dependent nature of the backward beam displacement, which is an area for future investigation.

We now wish to compare these experimental results with theory. The theoretical Scholte–Stoneley wave frequency, f_{SSt}, calculated for an angle of incidence of 22.5° is equal to 5.99 MHz. It can be seen in Fig. 5(a) that this frequency is within the bright high-amplitude zone at an angle of 21° and is in the null zone in the center of the specular beam. It is also a frequency contained within the trailing frequencies in the spectrogram of Fig. 6(b), and it is close to the maximum amplitude of the detected backward propagating surface wave. Therefore, we conclude that it is reasonable to assume that this frequency is displaced backward with respect to the specular beam and that its displacement is due to a backward propagating Scholte–Stoneley wave.

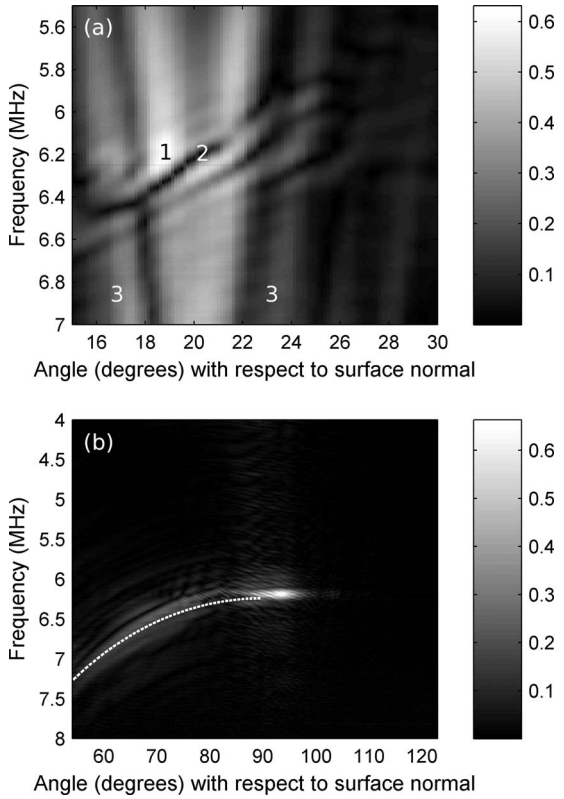

FIG. 7. (a) Angular spectrogram for a θ_i of 20° showing backward shifted frequencies in the region of specular reflection. (b) Complementary angular spectrogram showing the backward propagating Scholte–Stoneley wave and higher frequency propagating bulk modes (with theoretical locations shown by dotted line).

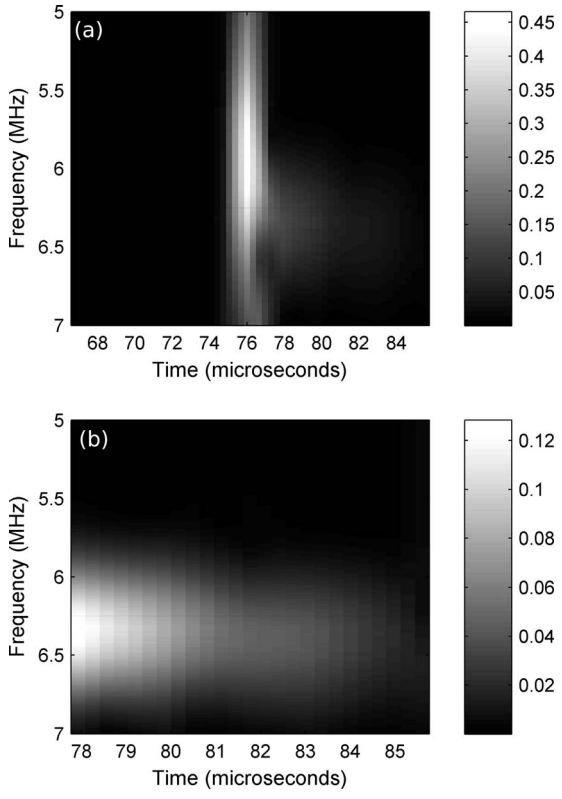

FIG. 8. (a) Classical spectrogram for a θ_i of 20° obtained from the time waveform captured at a receiver angle of 18.5°. (b) Close-up of the classical spectrogram in (a) to show the trailing frequencies arriving after the initial pulse.

B. Additional angles of incidence and associated frequencies

We now address results obtained for three additional angles of incidence, which are shown in Figs. 7–12 and are summarized in Table I along with the results previously discussed. For each case, Table I shows the appropriate figure numbers, the angle of incidence θ_i, the frequency of maximum amplitude found within the bright zone in each angular spectrogram, the range of frequencies found in the null zone of each angular spectrogram (amplitudes <0.1), the frequency of maximum amplitude in the trailing frequency band in each classical spectrogram (in all cases this frequency was found to remain the maximum over many time windows), the frequency of maximum amplitude of the backward propagating surface wave found in the complementary spectrogram of the region behind the emitting transducer, and the theoretical Scholte–Stoneley wave frequency f_{SSt}.

Concerning the scans in the regions of specular reflection, Figs. 7(a) and 9(a) exhibit features similar to those of Fig. 5(a), and the figures have been labeled in a similar manner. First, a bright zone of higher amplitude frequencies exists on the left side of each specular beam. The bright zone in Fig. 11(a) does not occur to the left of the specular beam, but rather inside it. This is attributed to the fact that as the angles of incidence and specular reflection increase, the projection of a backward displacement appears closer to the center of the receiving transducer. Figures 7(a) and 9(a) also show null zones of frequencies that can be found in the higher amplitude bright zone in the left side of the specular beam. For Fig. 11(a), the null zone has a different form because higher frequencies drop off sharply in the center of the specular beam. This can be attributed to the efficiency with which higher frequency propagating modes may be generated for these frequencies at this angle of incidence, as well as possible destructive interference occurring between these propagating modes and the specular beam. Therefore, the null zone for Fig. 11(a) has been calculated to occur where the frequencies drop off with amplitudes less than 0.1.

Classical spectrograms obtained from time waveforms captured during the scans in the regions of the specular beams are shown in Figs. 8, 10, and 12. Each figure contains a classical spectrogram obtained from a time waveform captured at an angular position to the left of the specular beam with the exception of Fig. 12. In this case, it appears that the measurement of the angle of incidence was at the upper limit of its uncertainty and the classical spectrogram was obtained from a time waveform received at an angle of 31.5°. In all the classical spectrograms, the specular beam arrival is seen as a vertical band of frequencies followed by trailing frequencies that are considered to be backward shifted frequencies, since they arrive after the initial pulse. Close-ups of the spectrograms more clearly reveal the range of frequencies that trail the initial pulse and there is a definite trend: the trailing frequencies of maximum amplitude decrease with increasing angle of incidence, and this is consistent with the other experimental results and with the theoretical Scholte–Stoneley wave frequencies. The wide bands of trailing fre-

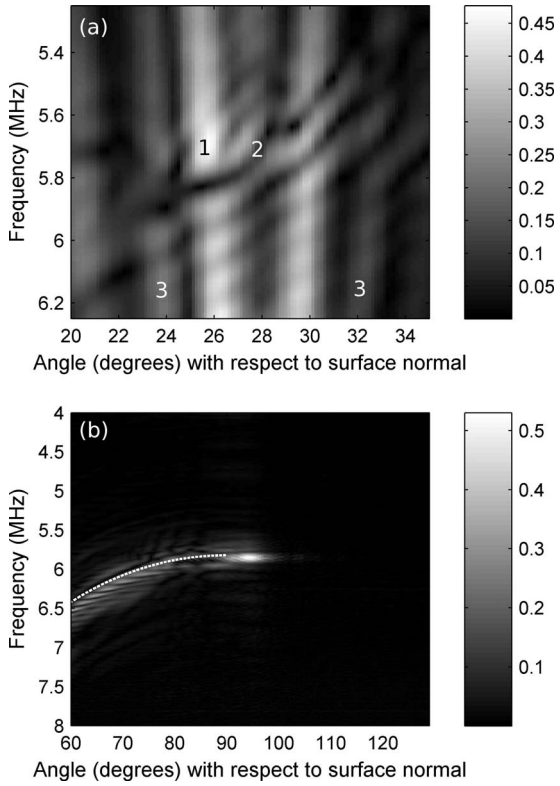

FIG. 9. (a) Angular spectrogram for a θ_i of 26.5° showing backward shifted frequencies in the region of specular reflection. (b) Complementary angular spectrogram showing the backward propagating Scholte–Stoneley wave and higher frequency propagating bulk modes (with theoretical locations shown by dotted line).

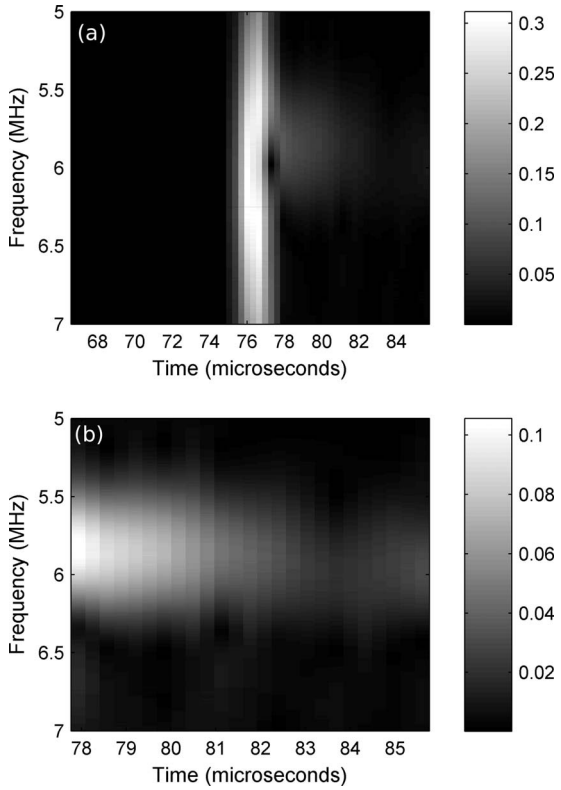

FIG. 10. (a) Classical spectrogram for a θ_i of 26.5° obtained from the time waveform captured at a receiver angle of 25.75°. (b) Close-up of the classical spectrogram in (a) to show the trailing frequencies arriving after the initial pulse.

quencies may suggest that when a pulse is incident on a periodically grooved surface, a range of backward shifted frequencies may be generated. One interesting feature found in all the classical spectrograms of Figs. 6(a), 8(a), 10(a), and 12(a) is a localized drop in amplitude for frequencies just below the trailing frequencies at the end of the specular beam arrival. The cause of this feature is unknown at this time, but it clearly has a time-dependent nature and is related to the diffraction occurring on the surface.

Concerning the complementary scans performed in the regions of the backward propagating surface wave, shown in Figs. 7(b), 9(b), and 11(b), a lateral wave is indeed observed at the surface of the sample and in all cases, and the wave has propagated off the edge of the sample into the field of the receiving transducer. This evidence, along with the fact that the experimentally observed frequencies of this surface wave are consistent with the other experimental evidence of backward shifted frequencies and the theoretical Scholte–Stoneley frequencies (f_{SSt}) for each angle of incidence, supports the claim that a backward propagating Scholte–Stoneley wave accompanies and is responsible for backward displaced frequencies. In addition to the backward propagating Scholte–Stoneley wave, higher order propagating bulk modes are observed for each angle of incidence, and their locations are well-described by theory, as shown by each dotted line.

In summary, it can be seen from the Figs. 5–12 and from Table I that in general, for all the angles of incidence studied here, experimental evidence has been observed that supports the existence of the backward beam displacement for multiple angles of incidence and frequencies and provides more insight as to the cause of that displacement. The frequencies of maximum amplitude found in the bright zones of the angular spectrograms, which, for three of the four angles studied, were observed to the left of the specular beam, are in reasonable agreement with the theoretically predicted backward Scholte–Stoneley frequencies, f_{SSt}. Also, the frequency ranges of all the null zones observed in the angular spectrograms contain the frequency of maximum amplitude observed in the bright zone and usually the appropriate f_{SSt} for each angle of incidence. The frequencies of maximum amplitude observed in the trailing frequencies in the classical spectrograms were toward the high end of the frequency ranges for the null zones and slightly higher than the theoretically predicted f_{SSt}. However, the classical spectrograms showed a wide range of potentially backward shifted frequencies which supports the existence of bright and null zones for a range of frequencies as was observed. Finally, all the frequencies of maximum amplitude of the observed backward propagating surface waves were consistent with the other experimental results and were close to the theoretically predicted f_{SSt}. We would like to make the comment that the ability of the theory to predict the experimental results could be improved with more research into the nature of the evolution of the Scholte–Stoneley wave velocity with frequency (dispersion) and the corrugation periodicity and form.

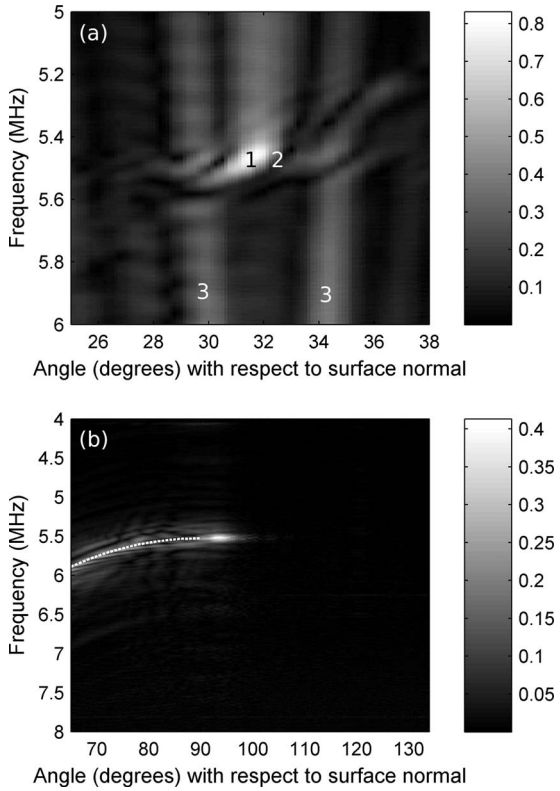

FIG. 11. (a) Angular spectrogram for a θ_i of 30.5° showing backward shifted frequencies in the region of specular reflection. (b) Complementary angular spectrogram showing the backward propagating Scholte–Stoneley wave and higher frequency propagating bulk modes (with theoretical locations shown by dotted line).

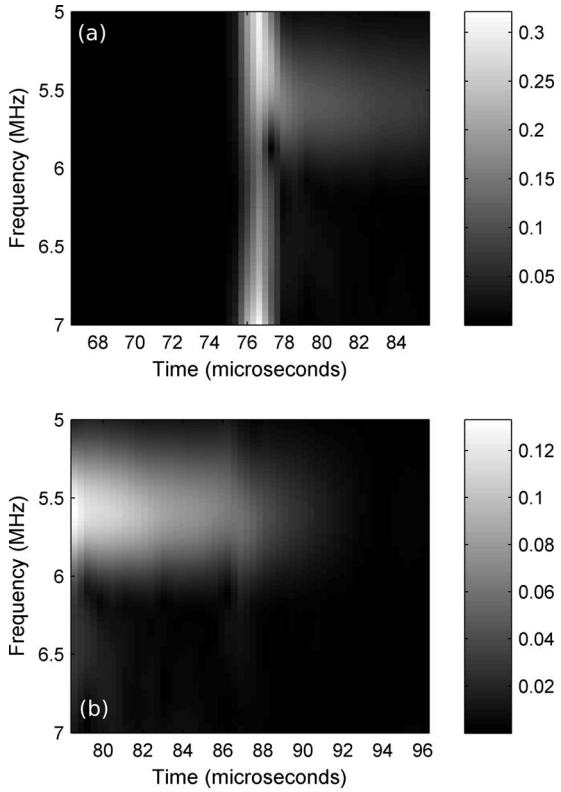

FIG. 12. (a) Classical spectrogram for a θ_i of 30.5° obtained from the time waveform captured at a receiver angle of 31.5°. (b) Close-up of the classical spectrogram in (a) to show the trailing frequencies arriving after the initial pulse.

These results lead us to conclude that the backward beam displacement can be observed for multiple angles of incidence and multiple frequencies, that the cause of the displacement is a backward propagating Scholte–Stoneley wave, and that the classical grating equation is a useful tool for predicting frequency and angle pairs that would result in the backward displacement.

V. CONCLUSIONS

New experiments concerning the ultrasonic backward beam displacement are reported in this work. Through the use of a pulse instead of a time-harmonic beam, it is possible to examine many frequencies at once. The two objectives of this work are to quantitatively show that the backward beam displacement exists at additional frequencies and angles of incidence other than the single frequency and angle of incidence pair (6 MHz, 22.5°) studied in the past and to show that the backward displacement is accompanied by a backward propagating Scholte–Stoneley wave. The experimental method employed in this work is first used to verify the original observations of Breazeale and Torbett and experimental results are then reported on additional angles of incidence where backward displaced frequencies and accompanying backward Scholte–Stoneley waves have been detected. The theory of Tamir and Bertoni[2] and the ability of the classical grating equation to predict the backward beam displacement as well as the propagation directions of bulk modes at multiple frequency and angle pairs are verified. It is possible, and highly likely, that the backward beam displacement is a continuous phenomenon that will occur for any frequency or angle of incidence on a periodically grooved solid, as long as the classical grating equation applies and is satisfied. These results have implications in the further study of periodic structures, for example, in the study of diffraction effects in phononic crystals.

TABLE I. Summary of results. Comparison of experimental observations and theoretical f_{SSt}.

Figures	Angle θ_i (deg)	Frequency of max amplitude in angular spectrogram (MHz)	Frequency range of null zone in angular spectrogram (MHz)	Trailing frequency of max amplitude in classical spectrogram (MHz)	Frequency of max amplitude of backward surface wave (MHz)	Theoretical f_{SSt} (MHz)
5 and 6	22.5	5.98	5.95–6.16	6.17	6.05	5.99
7 and 8	20	6.20	6.18–6.38	6.34	6.19	6.17
9 and 10	26.5	5.70	5.62–5.85	5.82	5.84	5.73
11 and 12	30.5	5.46	5.46–5.55	5.59	5.52	5.49

ACKNOWLEDGMENTS

The authors wish to acknowledge the French Centre Nationale de Recherche Scientifique (CNRS) and the Conseil Régional de Lorraine for their financial support of this work.

[1]M. A. Breazeale and M. A. Torbett, "Backward displacement of waves reflected from an interface having superimposed periodicity," Appl. Phys. Lett. **29**, 456–458 (1976).
[2]T. Tamir and H. L. Bertoni, "Lateral displacement of optical beams at multilayered and periodic structures," J. Opt. Soc. Am. **61**, 1397–1413 (1971).
[3]K. Mampaert and O. Leroy, "Reflection and transmission of normally incident ultrasonic waves on periodic solid-liquid interfaces," J. Acoust. Soc. Am. **83**, 1390–1398 (1988).
[4]J. V. Sánchez-Pérez, D. Caballero, R. Mártinez-Sala, C. Rubio, J. Sánchez-Dehesa, F. Meseguer, J. Llinares, and F. Gálvez, "Sound attenuation by a two-dimensional array of rigid cylinders," Phys. Rev. Lett. **80**, 5325–5328 (1998).
[5]V. Laude, M. Wilm, S. Benchabane, and A. Khelif, "Full band gap for surface acoustic waves in a piezoelectric phononic crystal," Phys. Rev. E **71**, 036607 (2005).
[6]B. Bonello, C. Charles, and F. Ganot, "Velocity of a SAW propagating in a 2D phononic crystal," Ultrasonics **44**, e1259–e1263 (2006).
[7]J. O. Vasseur, P. A. Deymier, G. Frantziskonis, G. Hong, B. Djafari-Rouhani, and L. Dobrzynski, "Experimental evidence for the existence of absolute acoustic band gaps in two-dimensional periodic composite media," J. Phys.: Condens. Matter **10**, 6051–6064 (1998).
[8]A. Khelif, A. Choujaa, S. Benchabane, B. Djafari-Rouhani, and V. Laude, "Guiding and bending of acoustic waves in highly confined phononic crystal waveguides," Appl. Phys. Lett. **84**, 4400–4402 (2004).
[9]C. Goffaux, F. Maseri, J. O. Vasseur, B. Djafari-Rouhani, and Ph. Lambin, "Measurements and calculations of the sound attenuation by a phononic band gap structure suitable for an insulating partition application," Appl. Phys. Lett. **83**, 281–283 (2003).
[10]T. Kundu, S. Banerjee, and K. V. Jata, "An experimental investigation of guided wave propagation in corrugated plates showing stop bands and pass bands," J. Acoust. Soc. Am. **120**, 1217–1226 (2006).
[11]D. Leduc, B. Morvan, A.-C. Hladky, P. Pareige, and J. L. Izbicki, "Lamb wave propagation in a plate with a grooved surface with several spatial periodicities," Ultrasonics **44**, e1359–e1363 (2006).
[12]N. F. Declercq, J. Degrieck, R. Briers, and O. Leroy, "Theoretical verification of the backward displacement of waves reflected from an interface having superimposed periodicity," Appl. Phys. Lett. **82**, 2533–2534 (2003).
[13]N. F. Declercq, J. Degrieck, R. Briers, and O. Leroy, "Theory of the backward beam displacement on periodically corrugated surfaces and its relation to leaky Scholte-Stoneley waves," J. Appl. Phys. **96**, 6869–6877 (2004).
[14]A. Teklu, M. A. Breazeale, N. F. Declercq, R. D. Hasse, and M. S. McPherson, "Backward displacement of ultrasonic waves reflected from a periodically corrugated interface," J. Appl. Phys. **97**, 084904 (2005).
[15]A. G. Every, R. E. Vines, and J. P. Wolfe, "Observation of Scholte-like waves on the liquid-loaded surfaces of periodic structures," Ultrasonics **38**, 761–766 (2000).
[16]R. Briers, O. Leroy, and G. N. Shkerdin, "Conversion of a Stoneley wave at the extremity of a fluid loaded plate," J. Acoust. Soc. Am. **101**, 1347–1357 (1997).
[17]E. Lamkanfi, N. F. Declercq, W. Van Paepegem, and J. Degrieck, "Finite element analysis of transmission of leaky Rayleigh waves at the extremity of a fluid-loaded thick plate," J. Appl. Phys. **101**, 114907 (2007).
[18]N. F. Declercq, A. Teklu, M. A. Breazeale, R. Briers, O. Leroy, J. Degrieck, and G. N. Shkerdin, "Study of the scattering of leaky Rayleigh waves at the extremity of a fluid loaded thick plate," J. Appl. Phys. **96**, 5836–5840 (2004).
[19]A. Tinel and J. Duclos, "Diffraction and conversion of the Scholte-Stoneley wave at the extremity of a solid," J. Acoust. Soc. Am. **95**, 13–20 (1994).
[20]N. F. Declercq, J. Degrieck, and O. Leroy, "The double-sided ultrasonic beam displacement," Appl. Phys. Lett. **85**, 4234–4236 (2004).
[21]W. G. Neubauer and L. R. Dragonette, "Measurement of Rayleigh phase velocity and estimates of shear speed by schlieren visualization," J. Appl. Phys. **45**, 618–622 (1974).